Current Biology 23, 1046–1056, June 17, 2013 ©2013 Elsevier Ltd All rights reserved http://dx.doi.org/10.1016/j.cub.2013.04.057

Article

Dynamic Localization of G-Actin during Membrane Protrusion in Neuronal Motility

Chi Wai Lee,[1,3,4] Eric A. Vitriol,[1,3] Sangwoo Shim,[1] Ariel L. Wise,[1] Radhi P. Velayutham,[2] and James Q. Zheng[1,*]
[1]Departments of Cell Biology and Neurology, Center for Neurodegenerative Diseases
[2]Department of Neurosurgery, Winship Cancer Center
Emory University School of Medicine, Atlanta, GA 30322, USA

Summary

Background: Actin-based cell motility is fundamental for development, function, and malignant events in eukaryotic organisms. During neural development, axonal growth cones depend on rapid assembly and disassembly of actin filaments (F-actin) for their guided extension to specific targets for wiring. Monomeric globular actin (G-actin) is the building block for F-actin but is not considered to play a direct role in spatiotemporal control of actin dynamics in cell motility.
Results: Here we report that a pool of G-actin dynamically localizes to the leading edge of growth cones and neuroblastoma cells to spatially elevate the G-/F-actin ratio that drives membrane protrusion and cell movement. Loss of G-actin localization leads to the cessation and retraction of membrane protrusions. Moreover, G-actin localization occurs asymmetrically in growth cones during attractive turning. Finally, we identify the actin monomer-binding proteins profilin and thymosin β4 as key molecules that localize actin monomers to the leading edge of lamellipodia for their motility.
Conclusions: Our results suggest that dynamic localization of G-actin provides a novel mechanism to regulate the spatiotemporal actin dynamics underlying membrane protrusion in cell locomotion and growth cone chemotaxis.

Introduction

The cell's ability to sense the environment and move in a defined direction is fundamental not only for embryo and tissue development but also for a wide range of physiological responses such as immunity and wound healing. Directional cell movement also constitutes a crucial step in many pathological events such as cancer cell metastasis. During brain development, directed neuronal migration sets up the laminar layers for the ordered brain architecture [1]. Led by the motile growth cone, guided extension of axonal fibers enables the precise wiring of intricate neuronal circuitry [2–4]. Both cell locomotion and growth cone migration utilize a shared mechanism in which actin-based membrane protrusion drives directed movement [5, 6]. The dynamic assembly and disassembly of actin filaments (F-actin) from globular actin (G-actin) generate lamellipodia and filopodial protrusions that, coupled with myosin motor-based retrograde transport and selective clutch engagement with the focal adhesions, steer and drive the cell or growth cone forward [5, 7]. The actin cytoskeleton is targeted by many signaling cascades, and a complex network of actin accessory molecules is known to act on distinct aspects of filament assembly, disassembly, and their organization into distinct networks for various cellular functions [8–10]. However, how these regulatory mechanisms cooperate to control actin-based cell protrusions remains to be fully understood.

G-actin is the building block for F-actin, and its local concentration directly impacts the filament assembly rate. Lamellipodia are known to contain G-actin [11, 12], but it is unknown whether it is spatiotemporally regulated there to play a functional role in cell migration. In this study, we examined the spatiotemporal distribution of G-actin in motile nerve growth cones and cells. We now provide direct evidence that a pool of G-actin is dynamically and spatially localized to the leading edge, creating sites of high G-/F-actin ratio that promote lamellipodia protrusions. Importantly, loss of the G-/F-actin ratio is tightly associated with cessation and retraction of membrane protrusions. We further show that the actin monomer-binding proteins profilin1 (Pfn1) and thymosin β4 (Tβ4) are involved in the spatial pattern of G-actin localization to the lamellipodia. Finally, a gradient of extracellular guidance cues can regulate G-actin localization, resulting in an asymmetry in the G-/F-actin ratio across the growth cone for directional steering. These findings suggest a novel mechanism by which G-actin and its spatiotemporal localization regulate the actin dynamics underlying localized lamellipodia protrusions of motile growth cones and cells, which may play an important role in neuronal motility during development.

Results

G-Actin Localizes to the Leading Edge of Lamellipodia

We used vitamin D-binding protein (DBP) to label G-actin [13, 14] and fluorescent phalloidin to label F-actin. We first examined *Xenopus* growth cones because they feature an actin-enriched peripheral region (P region) consisting of hallmark membrane protrusions of lamellipodia and filopodia [5, 6, 15]. Although both DBP and phalloidin labeled actin structures in the growth cone, they showed distinct spatial patterns. DBP staining was more enriched in the outer margin of the growth cone P region (Figure 1A; see also top panels in Figure S1A available online). Ratiometric overlay of the DBP and phalloidin channels showed that their ratio (hereafter referred to as the G/F ratio) was much higher at the peripheral edge, with several G/F ratio "hot spots" (arrows in Figure 1A; Figure S1A). A similar G/F pattern was also detected by immunostaining using JLA20, an antibody recognizing nonfilamentous actin [16] (Figure S1A), and AC-15, an antibody that recognizes both F- and G-actin (Figure S1C). The peripheral enrichment of G/F ratio was also observed in the growth cones of cultured hippocampal neurons (Figure S1D). We also examined the G-actin signals against a volume marker, 5-(4,6-dichorotriazinyl) aminofluorescein (DTAF) [17] (referred to as the G/V ratio), and confirmed their peripheral localization (Figure S1B). The distinct spatial patterns of G- and F-actin

[3]These authors contributed equally to this work
[4]Present address: Department of Physiology, Yong Loo Lin School of Medicine, National University of Singapore, Singapore 117597, Singapore
*Correspondence: james.zheng@emory.edu

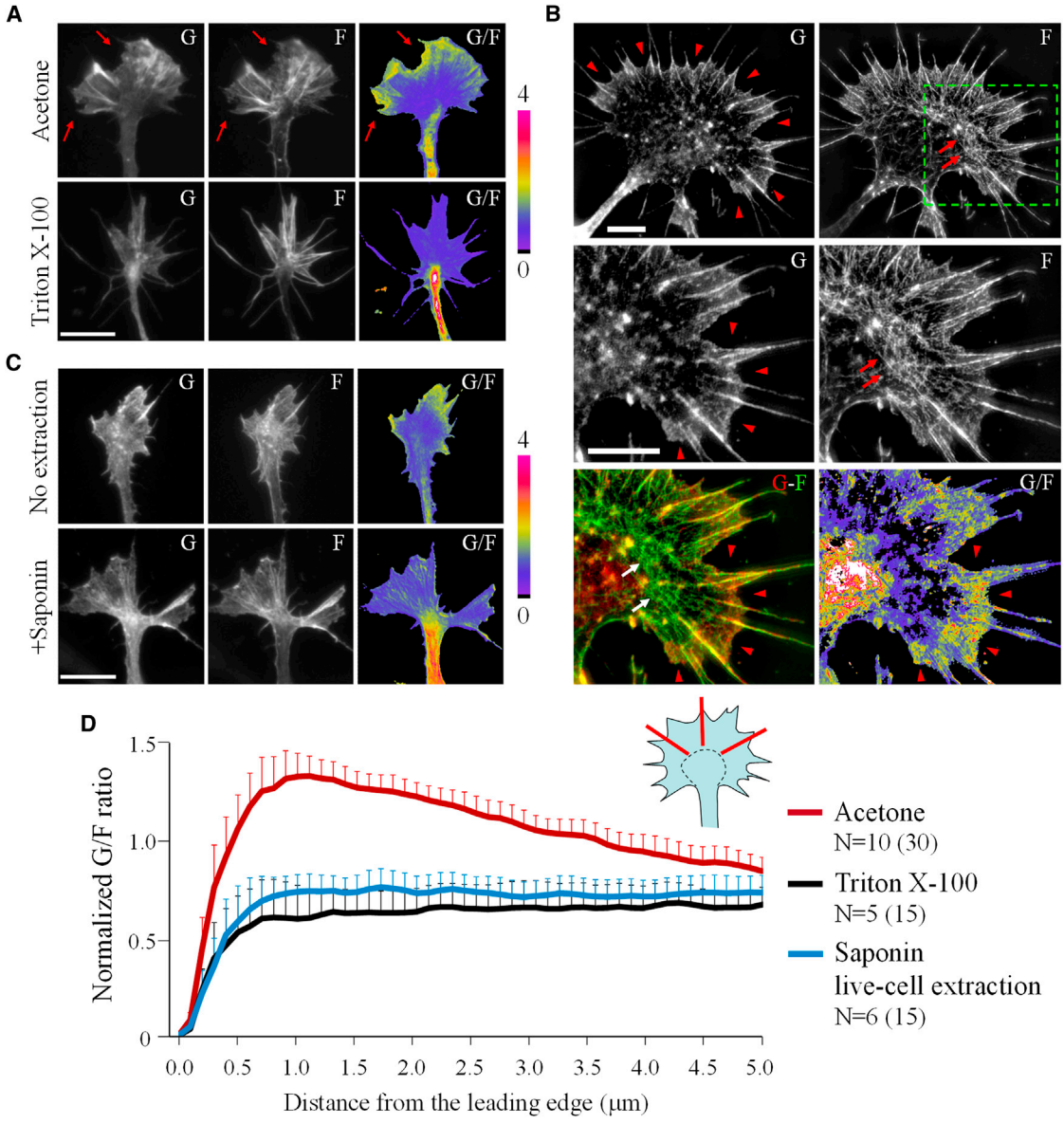

Figure 1. G-Actin Localization in Neuronal Growth Cones

(A–C) Representative images showing the differential localization of G- and F-actin in *Xenopus* growth cones labeled by DBP and fluorescent phalloidin, respectively. Scale bars represent 10 μm (A and C) and 5 μm (B).

(A) Growth cones permeabilized with cold acetone (top row) or Triton X-100 (bottom row) after fixation. Ratiometric images of G-/F-actin are shown in pseudocolors on the right. Red arrows indicate "hot spots" of high G/F ratio.

(B) SIM images of a *Xenopus* growth cone with the region indicated by the dashed green rectangle magnified (middle row) and shown on the bottom row as both a color overlay (G-F) and a ratio image of the two channels (G/F). Arrowheads indicate the enrichment of monomeric actin at the growth cone periphery. Arrows identify F-actin structures that were not labeled by DBP.

(C) *Xenopus* growth cones with (bottom row) and without (top row) a brief exposure to 0.02% saponin to extract actin monomers before they were fixed.

(D) Normalized line profiles depicting the local enrichment of G-actin at the leading edge of the lamellipodia of *Xenopus* growth cones stained for G-actin using acetone permeabilization (red line), saponin live-cell extraction followed by acetone permeabilization (blue line), or Triton X-100 permeabilization (black line). Error bars represent 95% confidence intervals. n indicates the number of cells (and number of lines) quantified.

For additional controls and labeling, see Figure S1.

were better resolved by structured illumination microscopy (SIM), which takes advantage of overlying moiré patterns of light to obtain spatial details beyond the diffraction limit [18]. A substantial pool of G-actin was found in the outer narrow margin of the growth cone lamellipodia (Figure 1B, arrowheads), whereas F-actin extends throughout the growth cone. Importantly, a majority of F-actin structures were not labeled by DBP (Figure 1B, arrows), indicating that DBP does not label F-actin in fixed cells.

The G-actin localization at the leading edge of growth cones was further supported by quantitative analysis of the G/F or G/V ratio using intensity line profiles of various actin probes (Figures 1D and S1A–S1C). It is of interest to note that the G-actin pattern revealed by DBP and JLA20 required the cells

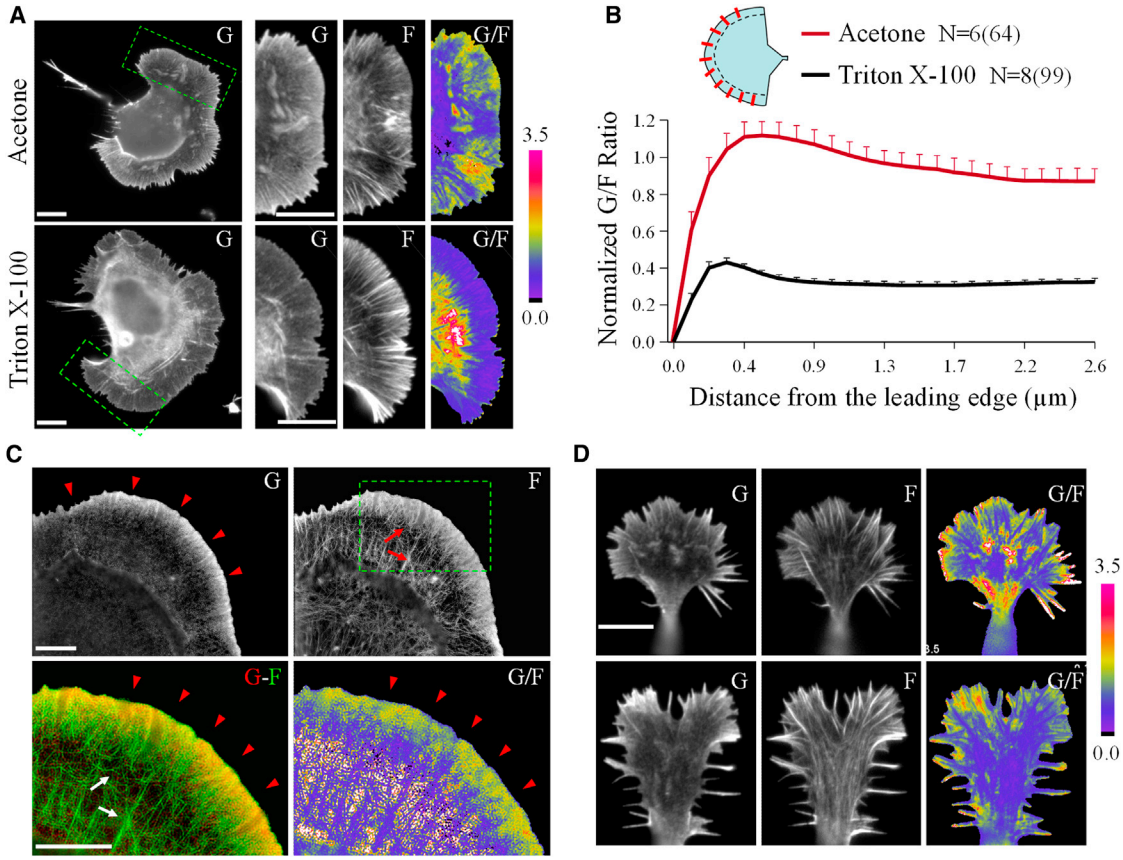

Figure 2. G-Actin Localizes in the Protrusions of Neuroblastoma Cells

(A) Representative images of CAD cells labeled with DBP and fluorescent phalloidin that were permeabilized with either acetone (top row) or Triton X-100 (bottom row). The areas enclosed by dashed green rectangles are shown in individual (G and F) and ratiometric (G/F) views. Scale bars represent 10 μm in (A) and (D) and 5 μm (C).

(B) Normalized line profiles depicting the local enrichment of G-actin at the leading edge of the lamellipodia of CAD cells permeabilized with either acetone or Triton X-100. Error bars represent 95% confidence intervals. n indicates the number of cells (and number of lines) quantified.

(C) SIM images revealing the differential localization of G- and F-actin in the lamellipodia of CAD cells. The region indicated by the dashed green rectangle is magnified and shown as a color overlay (G-F) and as ratio image of both channels (G/F). Arrowheads indicate the enrichment of nonfilamentous actin at the leading edge. Arrows identify F-actin structures that were not labeled by DBP.

(D) G-actin localization in the growth cones of differentiation-induced CAD cells. G-actin was labeled as in (A).

For control experiments verifying the specificity of G-actin probes, see Figure S2.

to be permeabilized by cold acetone after formaldehyde fixation. Use of 0.1% Triton X-100 eliminated the G-actin pattern without affecting F-actin staining by phalloidin (Figures 1A and 1D). Since Triton X-100 can extract soluble proteins in formaldehyde-fixed cells [19], this finding suggests that DBP and JLA20 labeling in the growth cone periphery highlighted a pool of G-actin that is highly labile and not part of the F-actin network. Similar results were also observed in motile Cath.a-differentiated (CAD) neuroblastoma cells [20] (Figures 2A and 2B). SIM images of DBP and phalloidin staining of CAD cell lamellipodia provided further support that DBP does not appear to label F-actin (Figure 2C, arrows) and that its signal is concentrated in the outer margin of the lamellipodia (Figure 2C, arrowheads). The high G/F ratio was also observed at the leading edge of the growth cones of CAD cells that underwent a differentiation protocol (Figure 2D) [20]. Therefore, G-actin localization to the leading edge of lamellipodia likely represents a common feature of motile membrane protrusions.

We confirmed the specificity of DBP and JLA20 for G-actin by four lines of evidence. First, both DBP and JLA20 staining was eliminated by adding purified G-actin to the labeling solution (Figure S2A). Second, actin filaments polymerized in vitro from rhodamine-conjugated G-actin (Rh-actin) were not labeled by DBP or JLA20 (Figure S2B). DNase I, another G-actin probe [21], was found to weakly label actin filaments in this in vitro preparation and thus was not used. Third, actin filaments polymerized in vitro from unlabeled G-actin were labeled by fluorescent phalloidin as well as by immunostaining using the anti-actin antibody AC-15, but not by DBP and JLA20 (Figure S2C). Finally, a brief live-cell extraction by saponin before fixation completely removed the peripherally localized G/F ratio by DBP (Figures 1C and 1D) or JLA20 (Figure S2C). Together, our labeling has specifically revealed the G-actin pattern.

Dynamic Localization of G-Actin Tightly Associates with Membrane Protrusion

To understand the dynamics and potential function of G-actin localization in cell protrusions, we performed simultaneous dual-channel live imaging on *Xenopus* spinal neurons

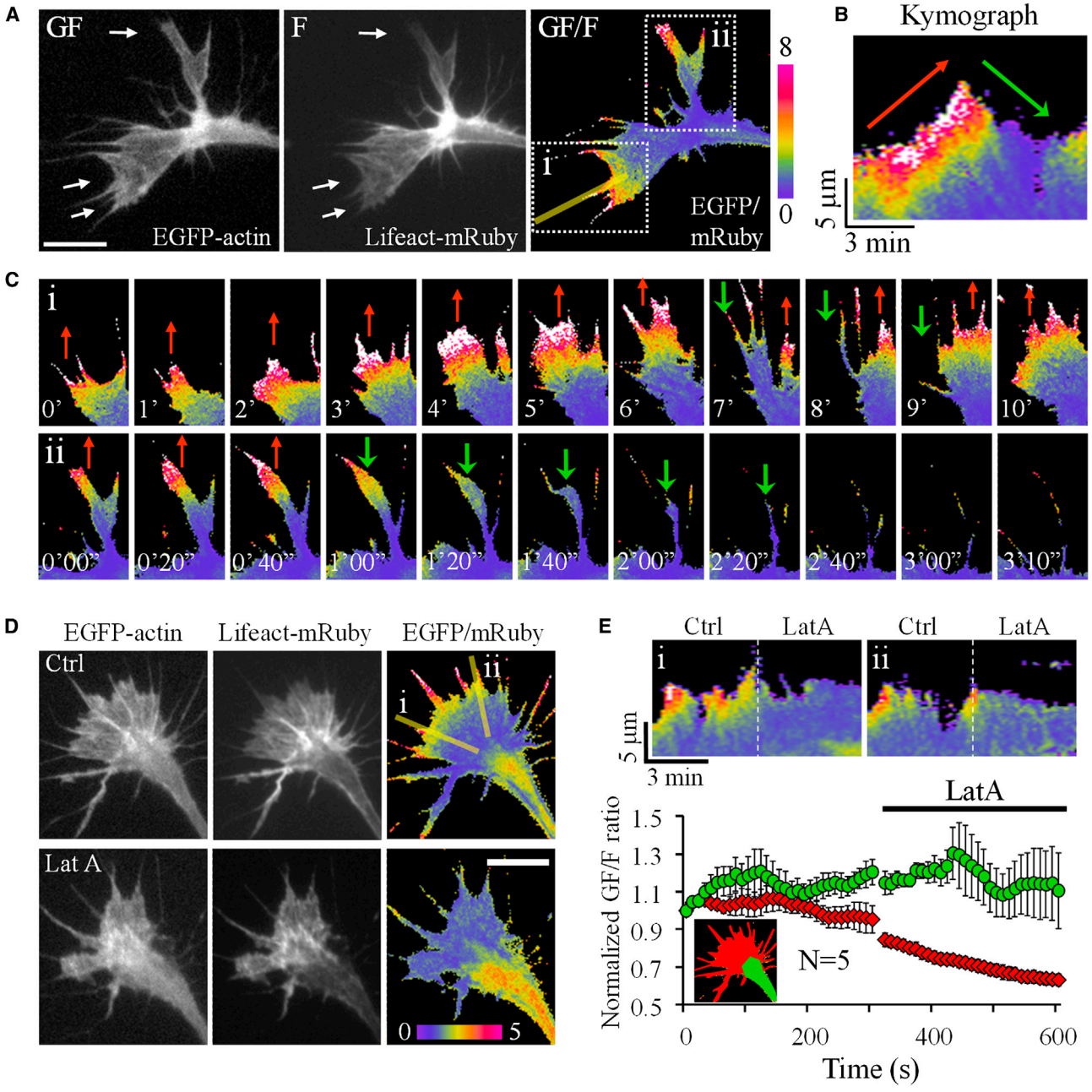

Figure 3. Dynamic Localization of G-Actin in Growth Cone Protrusion

(A–C) Dynamic G-actin localization in *Xenopus* growth cones as revealed by dual-channel time-lapse imaging of total (EGFP-actin) and filamentous (Lifeact-mRuby) forms of actin.

(A) Representative images of a *Xenopus* growth cone from 4–8 hr culture showing EGFP-actin, Lifeact-mRuby, and EGFP-actin/Lifeact-mRuby ratio images. Arrows indicate the protruding regions of the growth cone with a higher level of GFP-actin signals than that of Lifeact-mRuby.

(B) A kymograph constructed from the time-lapse sequence using the five-pixel line (yellow line in A).

(C) Montages of the time-lapse sequence from the two regions outlined by the dotted rectangles in (A). Red arrows, protruding; green arrows, retracting.

(D and E) Time-lapse series showing the elimination of G-actin by latrunculin A (LatA).

(D) Representative pairs of images showing EGFP-actin, Lifeact-mRuby, and their ratio in the same growth cone before and 5 min after LatA exposure.

(E) Kymographs constructed from two five-pixel-wide lines drawn across the growth cone periphery (yellow lines marked "i" and "ii" in D) showing the effects of LatA on G-actin localization and membrane protrusion. The plot shows the average GF/F ratio in the peripheral domain of the growth cone (red color) and central domain plus axonal shaft (green color) at different times before and after LatA treatment. Error bars represent the SEM.

Scale bars represent 10 μm. For additional data, see Figure S3 and Movies S1 and S3.

expressing EGFP-actin and Lifeact-mRuby. The EGFP-actin signal represents both G- and F-actin, whereas the short amino acid peptide Lifeact highlights F-actin inside the cell [22]. Both fluorescent probes labeled lamellipodia and filopodia (Figures 3A and S3A). Lifeact fluorescence completely overlapped with phalloidin labeling of the growth cone (Figure S3B), suggesting that the subset of F-actin unrecognized by Lifeact [23] is minimally present. When

compared with Lifeact-mRuby, EGFP-actin localized more intensely at the distal margin of growth cone lamellipodia (arrows in Figure 3A; see also Figure S3A). Ratiometric imaging of EGFP-actin/Lifeact-mRuby (hereafter also referred to as GF/F ratio) revealed regions of high GF/F ratio at the leading edge that appeared to undergo active protrusion. When analyzed using kymography (Figures 3B and S3C), the GF/F ratio indeed showed a marked elevation before and during the membrane protrusion (indicated by the red arrow), which dropped back to the baseline level when the protrusion ceased and started to withdraw (indicated by the green arrow). This tight coupling between the GF/F ratio and membrane protrusion can be better appreciated by montages created from the ratiometric time-lapse series (Figure 3C; see also Movie S1).

Without the supplement of neurotrophic factors, nerve growth cones lose their motility over time in culture and exhibit fewer lamellipodial protrusions [24, 25]. We found that *Xenopus* growth cones cultured for over 24 hr possessed mostly filopodia with little lamellipodia (Figure S3D). Local increase in the GF/F ratio was also observed coinciding with protrusions, but to a smaller extent in comparison to growth cones from 4–8 hr culture (Figures S3E and S3F; see also Movie S2). Furthermore, the gradual decline in both the GF/F ratio and growth cone extension rate over the course of 52 hr in culture (Figure S3G) suggests a connection between the basal GF/F ratio and growth cone motility.

To test whether the GF/F pattern highlighted the nonfilamentous pool of G-actin, we examined the effect of latrunculin A (LatA) on the GF/F ratio in *Xenopus* growth cones. LatA binds actin monomers to inhibit their polymerization [26] by affecting actin-monomer interface [27] and nucleotide exchange [28]. Exposure to a low concentration of LatA (20 nM) resulted in a rapid disappearance of the high GF/F ratio in the growth cone P region that coincided with a cessation of membrane protrusions (Figures 3D and 3E; Movie S3). A gradual elevation of GF/F ratio in the central region of the growth cone and the axonal shafts was observed after LatA treatment, suggesting that LatA-bound G-actin withdrew from the periphery to the central region of larger volume space (Figures 3D and 3E). These findings support the assumption that the GF/F ratio highlighted the nonfilamentous G-actin signals.

To better understand the dynamic localization of G-actin in cell motility, we examined the GF/F ratio in motile CAD cells to take advantage of their large and motile lamellipodia for high-resolution investigation. Consistent with the growth cone results, we observed a high GF/F ratio at the leading edge of membrane protrusions (Figure 4A). Quantitative analysis demonstrated that the high GF/F ratio was due to an increase in EGFP-actin fluorescence in the outmost margin of the lamellipodia rather than a decrease of Lifeact-mRuby (Figure 4A). Consistently, the elevated GF/F ratio was found to be tightly associated with the membrane protrusion, and its loss accompanied retraction (Figure 4B). To verify that the observed localization pattern of GF/F ratio was not an artifact resulting from a delay of Lifeact-mRuby in binding to newly formed actin filaments, we performed simultaneous fluorescence recovery after photobleaching (FRAP) to examine the recovery kinetics of both EGFP-actin and Lifeact-mRuby. Our data show that both probes exhibit similar recovery times (Figure 4C), arguing that Lifeact-mRuby is able to bind actin filaments in the lamellipodia as they are made. To verify that the increased EGFP-actin signal at the immediate cell edge represented a pool of unpolymerized G-actin, we performed live-cell extraction with saponin that can effectively remove monomeric EGFP-actin without affecting EGFP-actin incorporated into filaments [29]. Saponin extraction completely removed Lifeact-mRuby from the cell, which unfortunately prevented us from ratiometric imaging. However, we found that a brief exposure to saponin (0.02% for 1 min) resulted in a substantial reduction of the EGFP-actin signal at the leading edge, where the GF/F ratio was highest (Figure 4D). Since the high GF/F ratio is created by an elevated level of EGFP-actin (see the plot in Figure 4A), this result supports that our ratio imaging approach successfully highlights a labile pool of G-actin.

We next performed a series of experiments utilizing actin-specific drugs to further confirm the G-actin localization pattern in CAD cells. First, a low concentration of LatA (20 nM) eliminated the high GF/F ratio at the outer margin of the lamellipodia (Figure 5; Movie S4), similar to the results from growth cones. We also used jasplakinolide (Jasp) to stabilize F-actin and promote G-actin polymerization into F-actin [30]. A low concentration of Jasp (100 nM) substantially reduced the high GF/F ratio at the leading edge (Figure 5C; Movie S5). Importantly, both of these drug treatments perturbed the GF/F ratio without causing the lamellipodia to collapse. This low concentration of Jasp also effectively diminished the high GF/F ratio at the leading edge of *Xenopus* growth cones (Figure S4; see also Movie S6). Finally, cytochalasin D (CytoD), a mycotoxin that inhibits actin polymerization, reduced the high GF/F ratio at the leading edge at a relatively low concentration of 25 nM, but not at 2.5 nM (Figure 5C). At 100 nM CytoD, a large reduction in the GF/F ratio was observed (Figure 5C), but this was accompanied by a loss of F-actin and retraction of lamellipodia. Together, these results confirm that the GF/F ratio highlighted the G-actin pattern in living cells.

Profilin1 and Thymosin β4 in G-Actin Localization for Membrane Protrusion and Growth Cone Chemotaxis

To investigate the molecular mechanism of dynamic G-actin localization, we examined the involvement of profilin1 (Pfn1) and thymosin β4 (Tβ4), two well-known actin monomer-binding proteins [31, 32]. Lentivirus-based small hairpin RNAi (shRNAi) knockdown (KD) of both Pfn1 and Tβ4 in CAD cells resulted in a significant reduction of the GF/F ratio at the leading edge of the lamellipodia (Figures 6A and 6B). The effectiveness of knockdown was confirmed by RT-PCR and immunofluorescence (Figures S5A–S5C). Examining endogenous F-actin with phalloidin staining showed that Pfn1-KD lamellipodia had a marked reduction in size, whereas the Tβ4-KD lamellipodia appeared identical to the control (Figures 6C and 6D). Thus, while the Pfn1-KD cells demonstrated only a modest loss of G-actin localization in the lamellipodia (Figure 6B), they exhibited substantial defects in forming and/or maintaining the lamellipodial actin network. Tβ4-KD cells, however, displayed lamellipodia that were structurally indiscernible from wild-type cells by light microscopy. Kymograph analysis of time-lapse image sequences found that knockdown of Pfn1, not Tβ4, significantly reduced the protrusion velocity (Figures 6E and 6F). That Pfn1-deficient lamellipodia were not able to extend efficiently is consistent with their inability to properly assemble. Knockdown of either Pfn1 or Tβ4 severely impacted the protrusion extension distance and persistence time (Figure 6F). Thus, lamellipodia from Pfn1 and Tβ4 knockdown cells are unstable and collapse at much higher rates. These data suggest that G-actin localization,

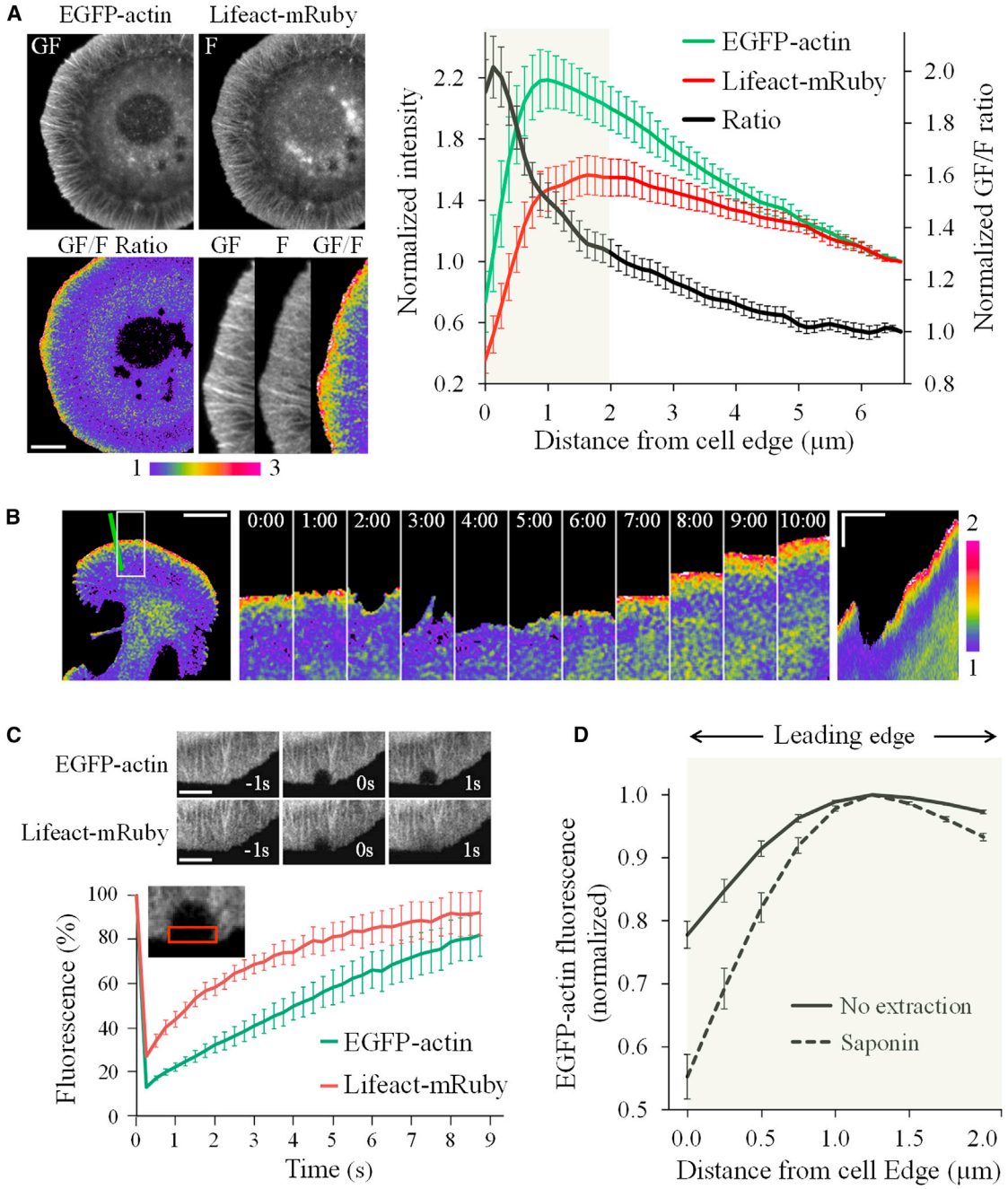

Figure 4. Dynamic Localization of G-Actin to the Leading Edge of Lamellipodia in Neuroblastoma Cells

(A) Representative images of a CAD cell expressing EGFP-actin and Lifeact-Ruby, and the EGFP-actin/Lifeact-mRuby ratio. The plot on the right depicts the results from linescan analysis for EGFP-actin (green), Lifeact-mRuby (red), and their ratio (black) profiles (n = 16 cells, 198 linescans). Error bars represent 95% confidence intervals. The light green shaded box indicates the distal region (2 μm wide) of the lamellipodia containing the high GF/F ratio. Scale bar represents 10 μm.

(B) A time-lapse sequence showing the tight association of elevated GF/F ratio and membrane protrusion. A CAD cell is shown in the leftmost panel (scale bar represents 10 μm), and a small region enclosed by the rectangle is depicted in the time-lapse montage. A kymograph was made from the green line indicated in the leftmost panel. The scale bars in the kymograph represent 5 min (horizontal) and 5 μm (vertical).

(C) Top: FRAP data showing the recovery rate of EGFP-actin and Lifeact-mRuby (n = 18). Representative images of both channels are shown above relative to the time they were photobleached (0 s). Bottom: quantification of the fluorescence recovery 1 μm from the leading edge is shown. Error bars represent 95% confidence intervals. Scale bar represents 5 μm.

(D) Linescan profiles of EGFP-actin fluorescence in CAD cells treated either with 0.02% saponin (saponin) or with a control buffer (no extraction) for 1 min prior to fixation. Cells treated with saponin (n = 15 cells, 153 linescans) showed a marked decrease in EGFP-actin intensity at the cell edge relative to cells that were not (n = 13 cells, 138 linescans). Error bars represent 95% confidence intervals.

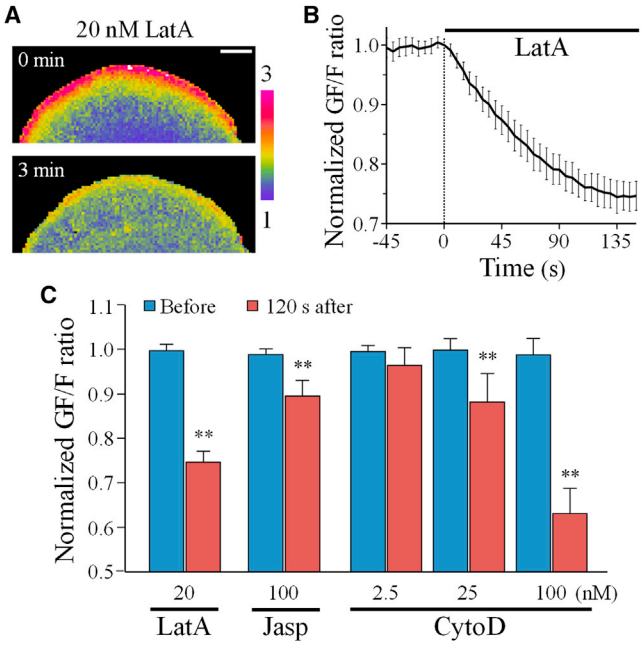

Figure 5. Effects of Actin Drugs on G-Actin Localization

(A) Representative ratio images of EGFP-actin and Lifeact-mRuby showing the effects of LatA on G-actin localization to the leading edge of CAD lamellipodia. Scale bar represents 10 μm.

(B) Normalized plot of GF/F ratio measured in a 5 μm-wide band at the leading edge of CAD cells treated with LatA (20 nM). Error bars in (B) and (C) represent 95% confidence intervals.

(C) Bar graph summarizing the results from different drug treatments. Note that while 100 nM cytocholasin D (CytoD) did cause an acute effect on the GF/F ratio, it was also accompanied by lamellipodia collapse and retraction. All other treatments shown did not induce retraction of the lamellipodia. **$p < 0.05$ (Student's t test). n = 9 (LatA), 7 (Jasp), 7 (2.5 nM CytoD), 7 (25 nM CytoD), and 5 (100 nM CytoD).

For additional data, see Figure S4 and Movies S4 and S5.

mediated by Pfn1 and Tβ4, plays a role in sustaining lamellipodial protrusions.

We next examined the GF/F ratio in nerve growth cones during attractive turning in response to a concentration gradient of bone morphogenetic protein 7 (BMP7) [33]. We found that *Xenopus* growth cones in 4–8 hr cultures responded to a BMP7 gradient with a local increase in G-actin on the side near the BMP7 source, which was detected before the turning of the growth cone (Figures 7A and 7C; Movie S7). Kymographs plotted across the near, central, and far side of the growth cone in respect to the local BMP7 application revealed the generation of protrusions on the near side in association with elevated GF/F ratio, whereas both GF/F ratio and protrusion on the far side were reduced (Figures 7B and 7D). Therefore, asymmetric G-actin localization and local increase in the G-/F-actin ratio may generate preferential actin-based lamellipodial protrusion to steer the growth cone.

Since Tβ4 was found to profoundly reduce both the lamellipodia GF/F ratio and the stability of membrane protrusions in CAD cells, we tested whether Tβ4 plays a role in growth cone turning in response to guidance cues. A morpholino antisense oligonucleotide against *Xenopus* Tβ4 (Tβ4-MO) was used for Tβ4 knockdown, which resulted in a substantial reduction (~30%) of Tβ4 in *Xenopus* neurons (Figures S5D and S5E). Consistently, the GF/F ratio in Tβ4-MO growth cones was significantly reduced (Figure 7E). We first performed neurite outgrowth assays and found that Tβ4 knockdown in *Xenopus* neurons resulted in enhanced neurite outgrowth after culturing for 7 hr (Figure 7F). Interestingly, however, *Xenopus* growth cones from Tβ4-MO-positive neurons no longer responded to the BMP7 gradient, whereas growth cones of control-MO neurons exhibited marked attraction (Figure 7G), as evidenced by the average turning angles (Figure 7H). The net extension of the growth cone over the 30 min turning assay, however, showed no difference, indicating that Tβ4-MO did not substantially alter the rate of growth cone extension during that short period of time. Therefore, Tβ4 may help to localize G-actin to the leading edge to function in directional responses that require persistent protrusion of lamellipodia and migration toward attractive cues.

Discussion

Actin filaments are polymerized from ATP-G-actin at the barbed end of existing filaments or nuclei and preferentially depolymerize at the pointed end as ADP-G-actin. A large pool of G-actin is prevented from spontaneous nucleation and polymerization by monomer-sequestering proteins [34]. As a result, the availability of polymerization-competent actin monomers at specific subcellular locations could directly impact local F-actin assembly. In both lamellipodia and filopodia, actin assembly occurs at the distal actin cytoskeleton-membrane interface where the limited space requires a mechanism to provide and sustain a pool of polymerization-competent actin monomers for actin polymerization. While passive diffusion is considered to supply actin monomers to the leading edge for assembly [10], studies using FRAP have estimated that the G-actin concentration in lamellipodia is much higher than previously thought, thus suggesting additional mechanisms [12]. Indeed, a rapid transport mechanism was suggested to shuffle actin monomers to the leading edge of lamellipodia [35], but direct support and its functional role remain missing. Our study here provides the first evidence that dynamic and spatiotemporal localization of G-actin plays an important role in membrane protrusion and cell motility. That the G-actin localization pattern was observed in motile growth cones and in the protrusions of migrating cells suggests that it represents a universal mechanism for actin-based motility.

The spatial pattern of G-actin localization in lamellipodia was confirmed by both staining of endogenous G-actin molecules using specific probes and live-cell imaging employing exogenously expressed EGFP-actin and Lifeact-mRuby. Importantly, live-cell imaging revealed the dynamics of G-actin localization and its association with the protrusive activity. It has been reported that EGFP-actin is unable to be incorporated into formin-nucleated actin filaments in the contractile ring of yeast cells [36]. Although formation of growth cone filopodia depends on formin [37], EGFP-actin appears to highlight F-actin in growth cone filopodia well in our study (see Figures 3A, 3D, and S3A). Importantly, we here focused on the lamellipodia, where EGFP-actin was well incorporated into the branched actin meshwork (see Figure 4A for example). Lifeact-mRuby also highlighted the same actin structures of *Xenopus* growth cones labeled by fluorescent phalloidin (Figure S3B), supporting the notion that Lifeact preferably labels F-actin in living cells [22]. Furthermore, we found that a different F-actin probe, F-tractin, which encodes a 66-amino acid sequence at the N terminus of phosphatidylinositol 3-kinase (PI3K) isoform A [38], highlighted the actin structures

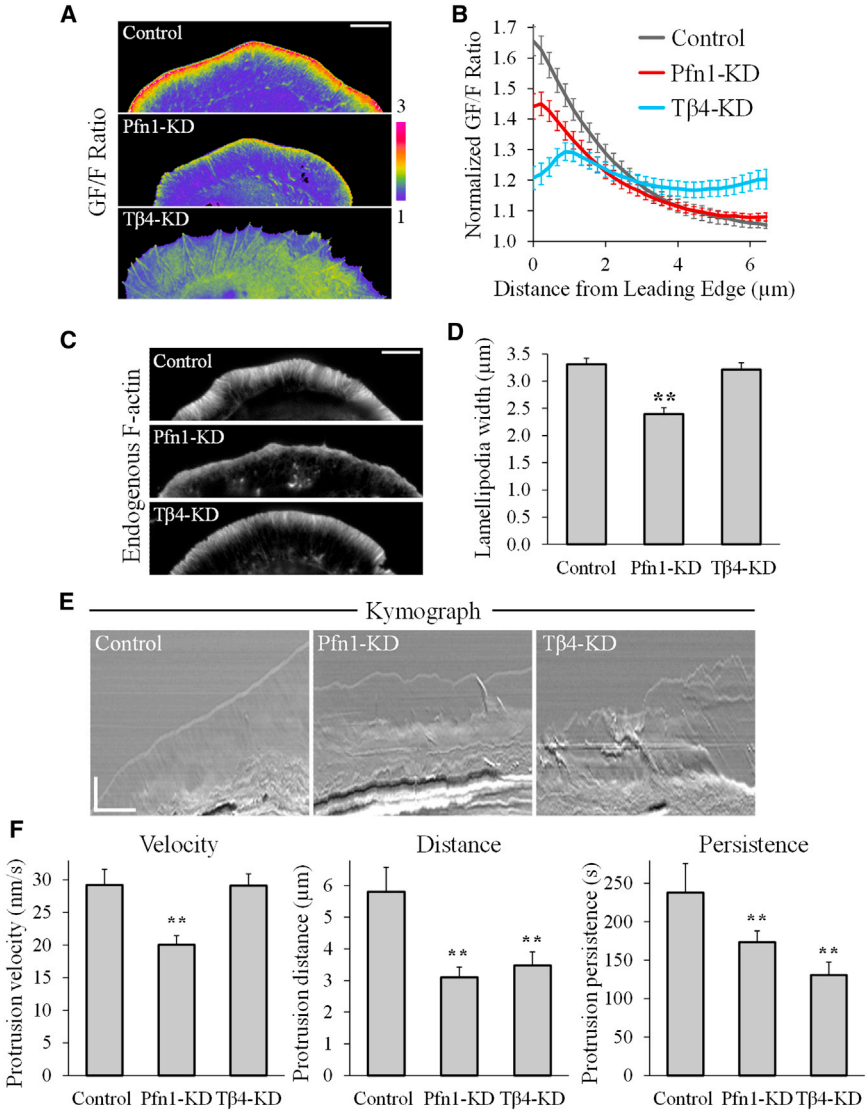

Figure 6. Profilin1 and Thymosin β4 Localize G-Actin and Regulate Protrusion Dynamics in Neuroblastoma Cells

(A) Representative images of the GF/F ratio in cells expressing scramble (control), profilin1 (Pfn1-KD), or thymosin β4 (Tβ4-KD) shRNAi. Scale bars in (A) and (C) represent 10 μm.

(B) Linescan analysis of the GF/F ratio in control, Pfn1-KD, and Tβ4-KD cells (15–18 cells and at least 140 linescans for each group). Error bars show 95% confidence intervals.

(C) Representative images of phalloidin labeling of control, Pfn1-KD, and Tβ4-KD cells.

(D) Bar graph depicting lamellipodia width of control, Pfn1-KD, and Tβ4-KD cells, measured as width of half-maximum from linescans of phalloidin-labeled cells (n = 16, 160 linescans). **p < 0.05 (Tukey's honestly significant difference [HSD] test).

(E) Representative kymographs from differential interference contrast time-lapse image sequences of control, Pfn1-KD, and Tβ4-KD cells. Scale bars represent 5 μm (vertical) and 5 min (horizontal).

(F) Bar graphs of kymograph analysis showing protrusion velocity (left), protrusion distance (middle), and protrusion persistence (right) for control, Pfn1-KD, and Tβ4-KD cells. n = 6 (149 protrusions), 6 (265 protrusions), and 5 (167 protrusions), respectively. Error bars show 95% confidence intervals. **p < 0.05 (Tukey's HSD test).

For the effectiveness of Pfn1 and Tβ4 knockdown in CAD cells, see Figures S5A–S5C.

identical to those of Lifeact (Figure S6A). Ratiometric imaging of EGFP-actin and F-tractin-tdTomato also showed an elevated GF/F ratio at the leading edge (Figures S6B and S6D). Finally, expression of Lifeact-EGFP and Lifeact-mRuby showed identical labeling of actin (Figure S6C). Together, these results suggest that the dynamic pattern of G-actin localization (depicted by GF/F ratio) is not a result of artifacts from the fluorescent probes used in this study.

Several families of G-actin-binding proteins may be involved in the subcellular localization of G-actin [34]. Here we found that Pfn1 and Tβ4 play an important role in the localization of G-actin at the leading edge of lamellipodia. These two G-actin-binding proteins have previously been shown to be involved in lamellipodial accumulation of G-actin in endothelial cells [39], although it is not known if they dynamically localize G-actin there to regulate protrusive activity and cell migration. Our results show that knockdown of Tβ4 essentially eliminated G-actin localization to the leading edge, resulting in lamellipodia that appeared structurally normal but were unstable and unable to extend efficiently. Pfn1 knockdown resulted in only a modest loss of G-actin localization but caused the lamellipodia to be structurally and dynamically affected (Figure 6). Profilin binds G-actin, promotes its nucleotide exchange for polymerization-competent ATP-G-actin, and delivers ATP-G-actin to the growing barbed end for assembly. Therefore, it is conceivable that its loss would markedly impact actin dynamics and membrane protrusion. Considering the number of actin regulators with which profilin interacts [40], it is difficult at this moment to pinpoint the mechanism underlying the lamellipodial effects observed with profilin1 knockdown. The disruption of *Xenopus* embryo development by profilin knockdown also prevented us from testing its role in directed migration of nerve growth cones [41, 42].

Tβ4 is mostly thought of as a passive buffer against polymerization. It is of interest to see that Tβ4 knockdown effectively eliminated G-actin localization at the leading edge of the lamellipodia and altered their protrusive dynamics. Interestingly, lamellipodia are able to form and extend normally in the absence of Tβ4, but they are unable to maintain that extension for productive forward movement. This phenotype could be explained by disrupted localization of G-actin to the leading edge, which would reduce the G-actin pool needed to sustain actin polymerization for persistent membrane protrusion. Moreover, the defects in lamellipodial protrusion (distance and persistence) caused by Tβ4 knockdown may also explain why Tβ4 is required for attractive turning of nerve growth cones, which depends on persistent lamellipodial protrusion toward the attractive source. The finding that Tβ4-MO neurons extended longer neurite processes than control cells

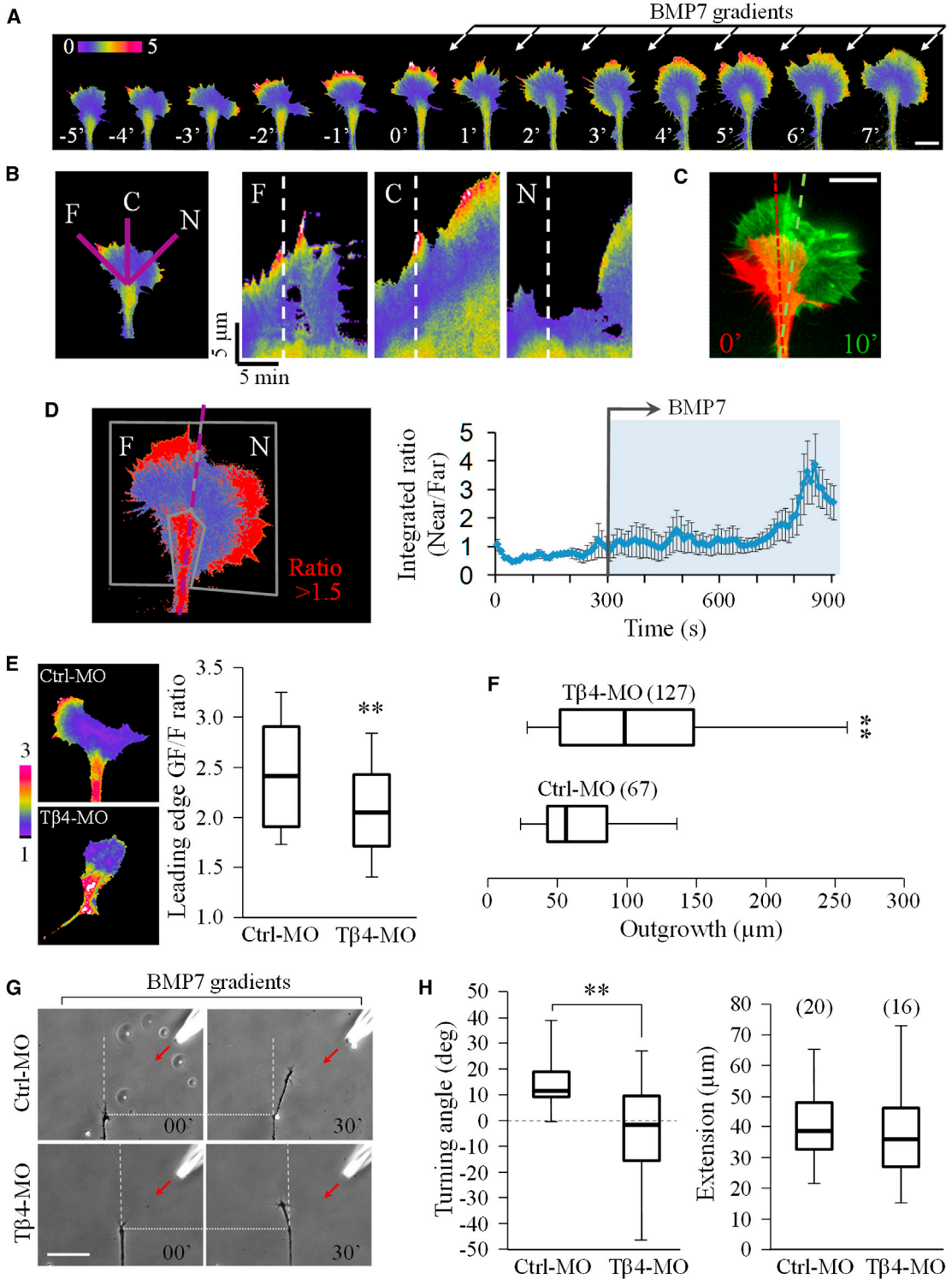

Figure 7. Dynamic Localization of G-Actin in Attractive Turning of Nerve Growth Cones

(A) Representative time-lapse GF/F images showing the asymmetric distribution of G-actin across the growth cone in response to local BMP7. Scale bars represent 10 μm in (A) and (B) and 50 μm in (G).

(B) Kymographs constructed from three five-pixel-wide lines placed at different locations of the growth cone in respect to the local BMP7: F, far; C, central; N, near.

(C) Superimposed EGFP-actin images at the beginning (red) and 10 min after local BMP7 application (green) showing the degree of growth cone turning. Dashed lines indicate the central axes of the growth cone at different time points.

(D) Quantitative data averaged from five growth cones showing the asymmetric distribution of G-actin in response to local BMP7. Error bars represent the SEM.

(legend continued on next page)

(Figure 7F) highlights two important points: (1) the effect on growth cone attraction is not a result of unselective disruption of growth cone motility, and (2) Tβ4 is dispensable for overall axon growth and formation of the growth cone lamellipodia. A role for Tβ4 in axon development is further supported by the finding that antisense knockdown of Tβ4 impaired axonal tract formation in zebrafish [43]. It will be of great interest to identify the upstream signals that direct a small pool of Tβ4-associated G-actin to localize to the leading edge during guidance.

Clearly, the mechanism proposed here is far from complete and will most likely involve concerted actions from other actin regulatory molecules. For example, G-actin is known to be recycled from existing filaments by depolymerization at the pointed end by the actin-depolymerizing factor (ADF)/cofilin. Jasp inhibits ADF/cofilin from binding actin filaments [44], which could explain the partial loss of localized actin monomers to the leading edge after Jasp addition. ADP-G-actin is believed to be rapidly trafficked to the polymerization site, converted to ATP-actin through nucleotide exchange factors, and added to the barbed end for filament elongation by a number of binding proteins [34]. Intriguingly, the observed G-actin localization pattern may represent a localized pool of polymerization-competent actin. LatA is known to inhibit nucleotide exchange of actin subunits, and its effect on G-actin localization suggests that the nucleotide state of actin monomers may be involved in their localization to the leading edge of lamellipodia. Actin localization may also be facilitated by motor-based transport such as myosin1c [45]. Also, the Arp2/3 complex-activating n-WASp WH2 domains bind G-actin and may function in the growth of dendritic actin filaments and their membrane associations for membrane protrusion [46]. We do know that G-actin localization occurs independently from protein translation, because protein synthesis inhibitors did not affect the G-/F-actin ratio (Figure S7). Therefore, future studies are clearly required to fully understand the mechanism and functions of G-actin trafficking to the leading edge. Nonetheless, our findings provide evidence for a novel mechanism by which dynamic localization of G-actin mediates spatiotemporally restricted actin-based membrane protrusion underlying directional cell motility.

Experimental Procedures

All experiments involving *Xenopus* frogs and embryos were carried out in accordance with NIH guidelines for animal use and were approved by the Institutional Animal Care and Use Committee of Emory University. *Xenopus* spinal neuron cultures, microinjection of DNAs and mRNAs, and turning assays were performed as previously described [33, 47]. To label G-actin, *Xenopus* neurons were fixed with 4% paraformaldehyde for 15 min, followed by 5 min exposure to cold acetone at −20°C [14] or 0.1% Triton X-100 for 10 min. Live-cell extraction was performed with 0.02% saponin (Sigma-Aldrich) for 10 s in permeabilization buffer (20 mM HEPES, 138 mM KCl, 4 mM $MgCl_2$, 3 mM EGTA, 1 mM ATP, and 1% BSA [pH 7.4]) before fixation. G-actin was labeled by DBP (Calbiochem) [14] or JLA20 anti-actin antibody (Calbiochem). F-actin was labeled by Alexa 488-conjugated phalloidin (Invitrogen), and volume labeling was performed using DTAF (Invitrogen).

Imaging of *Xenopus* neurons was performed on an inverted microscope (TE2000; Nikon) using a 60× 1.4 numerical aperture (NA) Plan Apo objective lens. Dual-channel live-cell imaging was performed with the use of a multispectral imager (Dual-View; Optical Insights). CAD cell imaging was performed on a Nikon A1R laser scanning confocal microscope using a 60× 1.49 NA Apo total internal reflection fluorescence (TIRF) objective lens and NIS-Elements (Nikon) software. EGFP constructs were excited using the 488 nm laser line, and mRuby and tdTomato constructs were excited with the 561 nm laser line. Simultaneous FRAP of EGFP-actin and Lifeact-mRuby was performed by irradiating a 2 μm circular region of interest at the cell edge with the 488 and 561 nm lines at 100% power simultaneously for 65 ms. EGFP-actin extraction and experiments using actin drugs were performed on a Nikon Ti-Eclipse inverted microscope with a 60× 1.45 NA Apo TIRF objective lens, a Photometrics QuantEM electron-multiplying charge-coupled device (EM-CCD) camera, and NIS-Elements software. Superresolution imaging was performed on an Eclipse Ti-E inverted microscope with SIM illuminator and microscope enclosure using a 100× NA 1.49 CFI Apo TIRF objective lens (N-SIM; Nikon). Digital images were acquired with an iXon DU897 EM-CCD camera (Andor) through the use of NIS-Elements.

For complete details of the experimental procedures, please see Supplemental Experimental Procedures.

Supplemental Information

Supplemental Information includes seven figures, Supplemental Experimental Procedures, and seven movies and can be found with this article online at http://dx.doi.org/10.1016/j.cub.2013.04.057.

Acknowledgments

We would like to thank James R. Bamburg (Colorado State University–Fort Collins) for input and discussion on the manuscript and William Bement (University of Wisconsin–Madison) for the suggestion of the experiments involving actin drugs. We are grateful to Nikon Instruments for providing an N-SIM system for our superresolution imaging. This project is supported in part by research grants from National Institutes of Health to J.Q.Z., a research development grant from the Muscular Dystrophy Association to C.W.L., a F32 fellowship award from National Institutes of Health to E.A.V., and a National Institute of Neurological Disorders and Stroke core facilities grant (P30NS055077) to the Integrated Cellular Imaging Microscopy Core of Emory Neuroscience.

Received: March 6, 2013
Revised: April 19, 2013
Accepted: April 19, 2013
Published: June 6, 2013

References

1. Hatten, M.E. (1999). Central nervous system neuronal migration. Annu. Rev. Neurosci. *22*, 511–539.
2. Tessier-Lavigne, M., and Goodman, C.S. (1996). The molecular biology of axon guidance. Science *274*, 1123–1133.

(E) The GF/F ratio in *Xenopus* growth cones injected with a morpholino against Tβ4 (Tβ4-MO) or a control morpholino (Ctrl-MO). The bar graph on the right shows the normalized GF/F ratio values from the first micrometer of the cell edge for each group (Ctrl-MO: n = 7 cells, 58 linescans; Tβ4-MO: n = 9, 97 linescans). Error bars are 95% confidence intervals. All box-and-whisker plots denote 95th (top whisker), 75th (top edge of box), 25th (bottom edge of box), and 5th (bottom whisker) percentiles and the median (bold line).
(F) Box-and-whisker plots showing neurite outgrowth after 7 hr in culture for Tβ4-MO and Ctrl-MO neurons.
(G) Representative phase-contrast images of *Xenopus* growth cones from neurons injected with Ctrl-MO (top row) or Tβ4-MO (bottom row) before and after 30 min exposure to a BMP7 gradient (red arrows). Dashed lines indicate the original direction of growth cone extension, and the dotted lines indicate the position of the growth cone at the onset of turning assay.
(H) Box-and-whisker plots show turning angle (left, in degrees [deg]) and extension distance (right) from BMP7 attraction experiments.
Numbers in parentheses indicate the number of cells examined. **$p < 0.001$ (Student's t test). See Movie S7 for asymmetric GF/F pattern during growth cone turning and Figures S5D and S5E for the effectiveness of Tβ4 knockdown in *Xenopus* neurons.

3. Dickson, B.J. (2002). Molecular mechanisms of axon guidance. Science *298*, 1959–1964.
4. Charron, F., and Tessier-Lavigne, M. (2005). Novel brain wiring functions for classical morphogens: a role as graded positional cues in axon guidance. Development *132*, 2251–2262.
5. Lowery, L.A., and Van Vactor, D. (2009). The trip of the tip: understanding the growth cone machinery. Nat. Rev. Mol. Cell Biol. *10*, 332–343.
6. Rodriguez, O.C., Schaefer, A.W., Mandato, C.A., Forscher, P., Bement, W.M., and Waterman-Storer, C.M. (2003). Conserved microtubule-actin interactions in cell movement and morphogenesis. Nat. Cell Biol. *5*, 599–609.
7. Suter, D.M., and Forscher, P. (1998). An emerging link between cytoskeletal dynamics and cell adhesion molecules in growth cone guidance. Curr. Opin. Neurobiol. *8*, 106–116.
8. Chhabra, E.S., and Higgs, H.N. (2007). The many faces of actin: matching assembly factors with cellular structures. Nat. Cell Biol. *9*, 1110–1121.
9. Pollard, T.D., and Borisy, G.G. (2003). Cellular motility driven by assembly and disassembly of actin filaments. Cell *112*, 453–465.
10. Pollard, T.D., Blanchoin, L., and Mullins, R.D. (2000). Molecular mechanisms controlling actin filament dynamics in nonmuscle cells. Annu. Rev. Biophys. Biomol. Struct. *29*, 545–576.
11. Van Goor, D., Hyland, C., Schaefer, A.W., and Forscher, P. (2012). The role of actin turnover in retrograde actin network flow in neuronal growth cones. PLoS ONE *7*, e30959.
12. Koestler, S.A., Rottner, K., Lai, F., Block, J., Vinzenz, M., and Small, J.V. (2009). F- and G-actin concentrations in lamellipodia of moving cells. PLoS ONE *4*, e4810.
13. Van Baelen, H., Bouillon, R., and De Moor, P. (1980). Vitamin D-binding protein (Gc-globulin) binds actin. J. Biol. Chem. *255*, 2270–2272.
14. Cao, L.G., Fishkind, D.J., and Wang, Y.L. (1993). Localization and dynamics of nonfilamentous actin in cultured cells. J. Cell Biol. *123*, 173–181.
15. Vitriol, E.A., and Zheng, J.Q. (2012). Growth cone travel in space and time: the cellular ensemble of cytoskeleton, adhesion, and membrane. Neuron *73*, 1068–1081.
16. Lin, J.J. (1981). Monoclonal antibodies against myofibrillar components of rat skeletal muscle decorate the intermediate filaments of cultured cells. Proc. Natl. Acad. Sci. USA *78*, 2335–2339.
17. Schindelholz, B., and Reber, B.F. (1999). Quantitative estimation of F-actin in single growth cones. Methods *18*, 487–492.
18. Gustafsson, M.G. (2000). Surpassing the lateral resolution limit by a factor of two using structured illumination microscopy. J. Microsc. *198*, 82–87.
19. Melan, M.A., and Sluder, G. (1992). Redistribution and differential extraction of soluble proteins in permeabilized cultured cells. Implications for immunofluorescence microscopy. J. Cell Sci. *101*, 731–743.
20. Qi, Y., Wang, J.K., McMillian, M., and Chikaraishi, D.M. (1997). Characterization of a CNS cell line, CAD, in which morphological differentiation is initiated by serum deprivation. J. Neurosci. *17*, 1217–1225.
21. Hitchcock, S.E. (1980). Actin deoxyroboncuclease I interaction. Depolymerization and nucleotide exchange. J. Biol. Chem. *255*, 5668–5673.
22. Riedl, J., Crevenna, A.H., Kessenbrock, K., Yu, J.H., Neukirchen, D., Bista, M., Bradke, F., Jenne, D., Holak, T.A., Werb, Z., et al. (2008). Lifeact: a versatile marker to visualize F-actin. Nat. Methods *5*, 605–607.
23. Munsie, L.N., Caron, N., Desmond, C.R., and Truant, R. (2009). Lifeact cannot visualize some forms of stress-induced twisted F-actin. Nat. Methods *6*, 317.
24. Peng, H.B., Yang, J.F., Dai, Z., Lee, C.W., Hung, H.W., Feng, Z.H., and Ko, C.P. (2003). Differential effects of neurotrophins and schwann cell-derived signals on neuronal survival/growth and synaptogenesis. J. Neurosci. *23*, 5050–5060.
25. Ming, Gl., Lohof, A.M., and Zheng, J.Q. (1997). Acute morphogenic and chemotropic effects of neurotrophins on cultured embryonic *Xenopus* spinal neurons. J. Neurosci. *17*, 7860–7871.
26. Spector, I., Shochet, N.R., Kashman, Y., and Groweiss, A. (1983). Latrunculins: novel marine toxins that disrupt microfilament organization in cultured cells. Science *219*, 493–495.
27. Morton, W.M., Ayscough, K.R., and McLaughlin, P.J. (2000). Latrunculin alters the actin-monomer subunit interface to prevent polymerization. Nat. Cell Biol. *2*, 376–378.
28. Yarmola, E.G., Somasundaram, T., Boring, T.A., Spector, I., and Bubb, M.R. (2000). Actin-latrunculin A structure and function. Differential modulation of actin-binding protein function by latrunculin A. J. Biol. Chem. *275*, 28120–28127.
29. Watanabe, N., and Mitchison, T.J. (2002). Single-molecule speckle analysis of actin filament turnover in lamellipodia. Science *295*, 1083–1086.
30. Bubb, M.R., Senderowicz, A.M., Sausville, E.A., Duncan, K.L., and Korn, E.D. (1994). Jasplakinolide, a cytotoxic natural product, induces actin polymerization and competitively inhibits the binding of phalloidin to F-actin. J. Biol. Chem. *269*, 14869–14871.
31. Mannherz, H.G., and Hannappel, E. (2009). The beta-thymosins: intracellular and extracellular activities of a versatile actin binding protein family. Cell Motil. Cytoskeleton *66*, 839–851.
32. Yarmola, E.G., and Bubb, M.R. (2006). Profilin: emerging concepts and lingering misconceptions. Trends Biochem. Sci. *31*, 197–205.
33. Wen, Z., Han, L., Bamburg, J.R., Shim, S., Ming, G.L., and Zheng, J.Q. (2007). BMP gradients steer nerve growth cones by a balancing act of LIM kinase and Slingshot phosphatase on ADF/cofilin. J. Cell Biol. *178*, 107–119.
34. Paavilainen, V.O., Bertling, E., Falck, S., and Lappalainen, P. (2004). Regulation of cytoskeletal dynamics by actin-monomer-binding proteins. Trends Cell Biol. *14*, 386–394.
35. Zicha, D., Dobbie, I.M., Holt, M.R., Monypenny, J., Soong, D.Y., Gray, C., and Dunn, G.A. (2003). Rapid actin transport during cell protrusion. Science *300*, 142–145.
36. Wu, J.Q., and Pollard, T.D. (2005). Counting cytokinesis proteins globally and locally in fission yeast. Science *310*, 310–314.
37. Matusek, T., Gombos, R., Szécsényi, A., Sánchez-Soriano, N., Czibula, A., Pataki, C., Gedai, A., Prokop, A., Raskó, I., and Mihály, J. (2008). Formin proteins of the DAAM subfamily play a role during axon growth. J. Neurosci. *28*, 13310–13319.
38. Johnson, H.W., and Schell, M.J. (2009). Neuronal IP3 3-kinase is an F-actin-bundling protein: role in dendritic targeting and regulation of spine morphology. Mol. Biol. Cell *20*, 5166–5180.
39. Fan, Y., Gong, Y., Ghosh, P.K., Graham, L.M., and Fox, P.L. (2009). Spatial coordination of actin polymerization and ILK-Akt2 activity during endothelial cell migration. Dev. Cell *16*, 661–674.
40. Ding, Z., Bae, Y.H., and Roy, P. (2012). Molecular insights on context-specific role of profilin-1 in cell migration. Cell Adhes. Migr. *6*, 442–449.
41. Khadka, D.K., Liu, W., and Habas, R. (2009). Non-redundant roles for Profilin2 and Profilin1 during vertebrate gastrulation. Dev. Biol. *332*, 396–406.
42. Sato, A., Khadka, D.K., Liu, W., Bharti, R., Runnels, L.W., Dawid, I.B., and Habas, R. (2006). Profilin is an effector for Daam1 in non-canonical Wnt signaling and is required for vertebrate gastrulation. Development *133*, 4219–4231.
43. Roth, L.W., Bormann, P., Bonnet, A., and Reinhard, E. (1999). beta-thymosin is required for axonal tract formation in developing zebrafish brain. Development *126*, 1365–1374.
44. Tsuji, T., Miyoshi, T., Higashida, C., Narumiya, S., and Watanabe, N. (2009). An order of magnitude faster AIP1-associated actin disruption than nucleation by the Arp2/3 complex in lamellipodia. PLoS ONE *4*, e4921.
45. Fan, Y., Eswarappa, S.M., Hitomi, M., and Fox, P.L. (2012). Myo1c facilitates G-actin transport to the leading edge of migrating endothelial cells. J. Cell Biol. *198*, 47–55.
46. Co, C., Wong, D.T., Gierke, S., Chang, V., and Taunton, J. (2007). Mechanism of actin network attachment to moving membranes: barbed end capture by N-WASP WH2 domains. Cell *128*, 901–913.
47. Lee, C.W., Han, J., Bamburg, J.R., Han, L., Lynn, R., and Zheng, J.Q. (2009). Regulation of acetylcholine receptor clustering by ADF/cofilin-directed vesicular trafficking. Nat. Neurosci. *12*, 848–856.